Environmental Science and Pollution Research (2022) 29:11172–11184
https://doi.org/10.1007/s11356-021-16414-9

RESEARCH ARTICLE

Application of the experimental design in the optimization of a procedure for antimony (Sb) remediation in environmental samples employing mesoporous array

José Arnaldo Santana Costa[1] · Vinicius Câmara Costa[2] · Matheus Lima de Mello[3] · Caio Marcio Paranhos[1]

Received: 15 June 2021 / Accepted: 5 September 2021 / Published online: 16 September 2021

Abstract

This study describes the sustainable and eco-friendly synthesis of the silica-based mesoporous structure from the use of alternative amorphous silica extracted from rice husk ash (RHA). The mesoporous material was called MCM-48 (RHA), and its application as adsorbent to the antimony (Sb) remediation in environmental samples was tested. The adsorbent was prepared by an efficient and sustainable hydrothermal method, which exhibited an amorphous framework with type IV isotherms and type H1 hysteresis, and surface area, total pore volume, and pore diameter values of 820.9 $m^2\ g^{-1}$, 0.6 $cm^3\ g^{-1}$, and 3.7 nm, respectively. In addition, the MCM-48 (RHA) exhibited a three-dimensional cubic mesostructure (*Ia3d* space-group symmetry) with a narrow mesopore distribution, uniform spherical particles, and well-defined architecture. Multivariate optimization using a factorial design (2^4) was employed in the adsorption tests of Sb. The variables evaluated and the optimum conditions obtained were (i) adsorbent mass (45 mg); (ii) adsorption time (115 min); (iii) pH 2; and (iv) Sb initial concentration of 8 mol L^{-1}. In these conditions, we found a maximum adsorption efficiency of Sb in the order of 95%. The adsorbent material proposed in this study proved to be efficient for Sb remediation in water samples under different experimental conditions. A total of five samples were analyzed and Sb concentrations on the order of 8 ppm were added, in which a removal efficiency of Sb raging between 88 and 96% was obtained for the remediation in real samples. In addition, the low cost of the synthesis of MCM-48 (RHA) in combination with its high and fast adsorption capacities offers a great promise for wastewater remediation, which makes it very attractive for environmental approaches.

Keywords Nanostructured mesoporous material · Sustainable approach · Factorial design · Antimony remediation

Highlights
- The sustainable and eco-friendly synthesis of MCM-48 mesoporous arrays.
- Use of RHA as an alternative and inexpensive silicon source.
- The MCM-48 exhibited large surface area and total pore volume.
- The MCM-48 exhibited a high removal efficiency of Sb.

Responsible Editor: Ioannis A. Katsoyiannis

✉ José Arnaldo Santana Costa
josearnaldo23@yahoo.com.br

[1] CDMF, Polymer Laboratory, Department of Chemistry, Federal University of São Carlos, São Carlos, São Paulo 13565-905, Brazil

[2] Embrapa Instrumentation, São Carlos, São Paulo 13560-970, Brazil

[3] Group of Applied Instrumental Analysis, Department of Chemistry, Federal University of São Carlos, São Carlos, São Paulo 13565-905, Brazil

Introduction

Industrial waste, commonly thrown into aquatic environments, contains both inorganic and organic contaminants, representing a global concern for many countries (Akhil et al. 2021). Among the various inorganic contaminants, antimony (Sb) is considered non-biodegradable pollutant and that can cause many environmental damages. Furthermore, carcinogenic contaminants cause health problems, especially for human beings (Viczek et al. 2020). The main industrial activities that can contribute to the discharge of Sb in aquatic environments come from the industries of fire retardants, pigments, mining, and ceramics (Aquino et al. 2016; Chu et al. 2019; Meng et al. 2020). Some countries, such as China, Grace, and India, have suffered from problems of contamination in groundwater by Sb, which can cause damage to human health (Antoniadis

et al. 2019; Xu et al. 2019). In this sense, the development of methodologies that are efficient for the Sb remediation from wastewater is essential.

Among the various approaches in the literature for the Sb remediation (Xiang-Xue et al. 2019; Chen et al. 2020), adsorption technology is the most common method used, and several adsorbents have been developed (Zhao et al. 2010), mainly due to the various advantages presented by the adsorption technology, such as no generation of byproducts, easy operation and reusability, and low cost (de Jesus et al. 2021). Despite the various absorbent materials already available in the literature, it is still necessary to find an absorbent material that has the following characteristics: (i) low cost, eco-friendly, and sustainable; (ii) good physical and chemical stability; (iii) excellent textural and structural features; and (iv) high selectivity, so on (Costa and Paranhos 2020; Costa et al. 2020b). In this context, the synthesis of mesoporous materials has attracted a great deal of interest for the adsorption process and have already been used with success for the removal of the organic compounds (Santos et al. 2019; Costa et al. 2020c, d, 2021a, b) and inorganic constituents (de Sá et al. 2020; Costa et al. 2020a).

The mesoporous structures were synthesized for the first time in the early 1990s and have since been used in the most diverse technological applications, such as extraction methods (Santos et al. 2019; de Sá et al. 2020), biomedical approaches (Kankala et al. 2020), catalytic applications (Doustkhah et al. 2019), energy devices (Wang et al. 2018), and filler material in mixed matrix membranes (Costa et al. 2020c, 2021b). The best known and/or studied mesoporous materials are those of the M41S family, represented by MCM-41 (hexagonal phase), MCM-50 (lamellar phase), and MCM-48 (cubic phase) (Costa et al. 2015, 2017a, 2017b; Santos et al. 2019), which is the focus of this approach.

The mesoporous structures have attractive features, such as good thermal and mechanical stability, and high surface area, which allows the diffusion and/or adsorption process of the organic and inorganic compounds through their uniform pores and high mesoporous arrangement, as well as ease in the synthesis and functionalization process of these ordered structures (Costa et al. 2014, 2015, 2017a, 2017b; Saleh 2020; de Jesus et al. 2021). The silica-based mesoporous arrays are synthesized via the hydrothermal method from the use of a surfactant (directing agent), a catalyst (acid or basic), and mainly from a silica source, which is responsible for forming the framework of the amorphous material (Costa et al. 2015, 2017b, 2020e).

In the literature, there are several works showing the synthesis of these mesoporous materials from the use of the commercial silica sources, mainly tetraethylorthosilicate (TEOS) (Costa et al. 2014, 2017b; Ambursa et al. 2017), silica gel (Santos et al. 2019), and sodium silicate (Costa et al. 2017a, 2019a; Santos et al. 2019). However, there are some works that show the preparation of the mesoporous structures from the use of alternative, sustainable, and eco-friendly materials as a silica source, such as fly ash (Castillo et al. 2018), rape straw (Li et al. 2019), straw ash (Ma et al. 2016), bamboo leaf ash (Arumugam et al. 2018), rice husk (Sohrabnezhad and Daraie Mooshangaie 2019), sedge ash (Ghorbani et al. 2013), and sugarcane bagasse (Norsuraya et al. 2016). In the present approach, we use the rice husk ash (RHA) as an alternative, inexpensive, eco-friendly, low-cost, abundant, and accessible source of amorphous silica for the synthesis of the mesoporous material with a cubic phase (MCM-48 (RHA)), which was later used as an adsorbent material in the Sb removal in aqueous media.

Most of the approaches found in the literature, which are dedicated to the adsorption studies, are carried out from the univariate optimization of the adsorption tests, which aim at understanding the adsorption mechanism between the adsorbent material and the adsorbate, especially from the correlation of experimental adsorption data with kinetic and isothermal theoretical models (Costa et al. 2014; Costa and Paranhos 2019). However, these approaches are laborious and require expert analyst.

Recently, a demand has emerged for the optimization steps of the procedures that are fast and with a reduced number of experiments (Ferreira et al. 2018). In this sense, the multivariate optimization techniques have been shown powerful to evaluate the variables that affect the analytical response in order to obtain the best conditions of optimization to ensure the procedure reliability (Saleh et al. 2017, 2018; Adio et al. 2017). Among the multivariate optimization tools, factorial design is more employed and allows a preliminary evaluation of the variables for the development of linear models (Costa et al. 2019c; Gamela et al. 2020). These tools have numerous advantages, such as (i) possibility of evaluating synergistic and antagonistic interactions between variables; (ii) possibility of forecasting the system under study in a condition that has not been tested in practice; and (iii) reduction in the generation of chemical waste which contributes to the principles of green chemistry (Ferreira et al. 2017; Costa et al. 2018). Factorial designs have been used in several areas, but their use in adsorption procedures has not been explored sufficiently.

In this context, the factorial design was employed to optimize a procedure for Sb remediation in wastewater. In addition, the adsorbent material used was obtained from a cleaner, low-cost, and eco-friendly approach from the use of alternative amorphous silica extracted from RHA.

Experimental

Standards, solvents, and reagents

The rice husk (RH) of agulhinha (Indian origin) variety was received from the Brazilian Agricultural Research

Corporation (Embrapa) (São Carlos, São Paulo, Brazil). Details about thermal treatment realized to obtain RHA from RH and characterizations are available in the publication of Costa et al. (2018). Ultrapure water (18.2 MΩ cm^{-1} resistivity) produced by a Milli-Q® Plus Total Water System (Millipore Corp., Bedford, MA, USA) was used to prepare all the solutions. The Sb analytical standards (Qhemis, São Paulo, SP, Brazil), cetyltrimethylammonium bromide (CTAB) (Neon, Suzano, SP, Brazil), sodium hydroxide (NaOH) (Synth, Diadema, SP, Brazil), and hydrochloric acid (HCl) 37% w/v (Synth, Diadema, SP, Brazil) were used during the procedure. All materials were washed with soap and soaked in 10% v/v nitric acid (HNO_3) for 24 h. After that, a rinsing step with ultrapure water was performed, and the materials were left to dry in a clean hood before use.

Preparation of MCM-48 (RHA) mesoporous array

The mesoporous array (named MCM-48 (RHA)) was synthesized from RHA of the agulhinha variety. Thus, amorphous silica was extracted from the RHA by leaching with sodium hydroxide solution and the MCM-48 (RHA) was synthesized by a hydrothermal route. The extraction of the sodium silicate solution was performed according to our methodology developed recently (Costa and Paranhos 2018): Briefly, the RHA (10 g) was dissolved in NaOH solution (100 mL) in constant agitation (80 °C, 1 h). After the reaction period, the sodium silicate solution obtained was filtered (i) through quantitative filter paper (12 μm) and (ii) through quantitative blue band filter paper (8 μm), and then it was transferred to a sealed polypropylene flask at room temperature.

The MCM-48 (RHA) was synthesized as follows: (i) initially, 10 g of CTAB was dissolved in 70 mL of NaOH solution (0.75 mol L^{-1}) under constant stirring at room temperature for 1 h; (ii) after this time, 50 mL of the sodium silicate solution from RHA was added slowly into the solution; (iii) later, this mixture was stirred at room temperature for 2 h and then transferred to a Teflon-lined stainless steel autoclave, which was placed in a vacuum oven and heated at 100 °C for 48 h; (iv) after this time, the solution pH was adjusted to ~10 with HCl solution (1 mol L^{-1}) and the reactor was left in the oven for another 24 h at 100 °C; (v) the solid product obtained was filtered, washed with deionized water, and dried in a vacuum oven at 100 °C for 12 h; (vi) finally, CTAB removal was performed by calcination at 550 °C for 6 h at a rate of 1 °C min^{-1}.

Characterization of MCM-48 (RHA) adsorbent

The characterization of the RH and RHA was complemented using scanning electron microscopy-energy dispersive X-ray spectroscopy (SEM-EDS). SEM analysis was achieved in a FEG-XL30 (Philips) equipment with an EDS accessory, operating with the help of a secondary electron (SE) detector and an accelerator power of at 3 kV. The prepared MCM-48 (RHA) was characterized using Fourier transform infrared spectroscopy (FTIR) spectra for powder samples in the form of KBr pastilles achieved in the region of 4000 to 400 cm^{-1} using a Varian 3100 equipment (at room temperature, 32 scans, and a resolution of 4 cm^{-1}). Powder X-ray diffractometry (XRD) analysis was performed on a LabX XDR-6000 (Shimadzu) equipment using Cu Kα radiation source (λ = 1.5406 Å) at a voltage/current display of 30 kV/30 mA. The data were collected with a diffraction angle (2θ) ranging from 5 to 80° and a scanning rate of 2° min^{-1}. Nitrogen adsorption and desorption isotherms of MCM-48 (RHA) (~100 mg was evacuated for 2 h at 150 °C) were acquired using a NOVA 1200 apparatus at liquid nitrogen temperature (−196.15 °C). Additionally, the surface area (S_{BET}) and the pore size distribution (D_{BJH}) values were calculated from the adsorption data, using the Brunauer-Emmentt-Teller and the Barrett-Joyner-Halenda methods, respectively.

Determination of the Sb

The Sb concentrations were measured using an inductively coupled plasma optical emission spectrometry (ICP OES) (iCAP 7000, Thermo Scientific, Waltham, MA, USA). Argon gas (99.996%, White Martins-Praxair, Sertãozinho, SP, Brazil) was used to generate the plasma in all ICP OES measurements. The instrumental conditions were established as the manufacturer recommendations as follows: power: 1.2 kW, plasma gas flow: 15.0 L min^{-1}, auxiliary gas flow: 1.5 L min^{-1}, nebulizer gas flow: 0.7 L min^{-1}, sample introduction flow rate: 2.1 mL min^{-1}. The emission lines monitored were Sb 206.8 and 231.1 nm.

Multivariate optimization of adsorption procedure

A full factorial design (2^4) was used in order to optimize experimental conditions of the adsorption procedure for Sb removal from wastewater. In this study, the variables were evaluated in three levels including the central point: (i) solution pH (2, 6, and 10), (ii) adsorption time (5, 60, and 115 min), (iii) concentration of the Sb standard (2.0, 5.0, and 8.0 mg L^{-1}), and (iv) adsorbent mass (5, 25, and 45 mg). A total of 19 experiments were carried including triplicate in the central point, which was used to estimate the pure error. A response to full factorial design (2^4) was calculated % removal of Sb, obtained from Eq. 1:

$$\%\text{removal of Sb} = \frac{(C_0 - C_e)}{C_0} \times 100$$

where C_0 and C_e (mg L^{-1}) are the initial and equilibrium concentrations of Sb, respectively.

Adsorption experiments were conducted in amber flasks (25 °C, 400 rpm) in 5 mL of Sb solution. After the adsorption process, the samples were centrifuged (3500 rpm, 5 min), and then the supernatant concentration was performed using an ICP OES.

Results and discussion

As mentioned before, all characterizations of the RH and RHA were performed in our recently published article in the literature (Costa and Paranhos 2018); however, this characterization was complemented by SEM-EDS analysis.

Characterization of MCM-48 (RHA) adsorbent

Figure 1a illustrates the FTIR spectra obtained for the MCM-48 (RHA) mesoporous array before and after the CTAB removal. The MCM-48 (RHA) with CTAB presents the narrow bands centered at 2921 and 2852 cm^{-1}, which are attributed to the stretching of C−H bond, and at 1485 cm^{-1} related to the deformation of C−H bond of CH_2 and CH_3 groups of the CTAB surfactant (Costa et al. 2014; Fitaroni et al. 2019). However, these bands are absent in the calcined MCM-48 (RHA) (Santos et al. 2019). It is also possible to observe for both samples a broad band at 3443 cm^{-1}, which can be attributed to the vibrational modes of stretching of O−H bond of silanol (Si−OH) groups, as well as to the H_2O molecules adsorbed on the surface of the MCM-48 (RHA) (Jang et al. 2009; Saleh 2018), and also a narrow band at 1634 cm^{-1} is attributed to the bending vibration of H_2O molecules trapped within the mesoporous matrix of the MCM-48 (RHA). Finally, it is possible to observe the main bands associated with the cubic structure of the MCM-48 (RHA), confirmed by the bands located at 1089 cm^{-1} attributed to the asymmetric

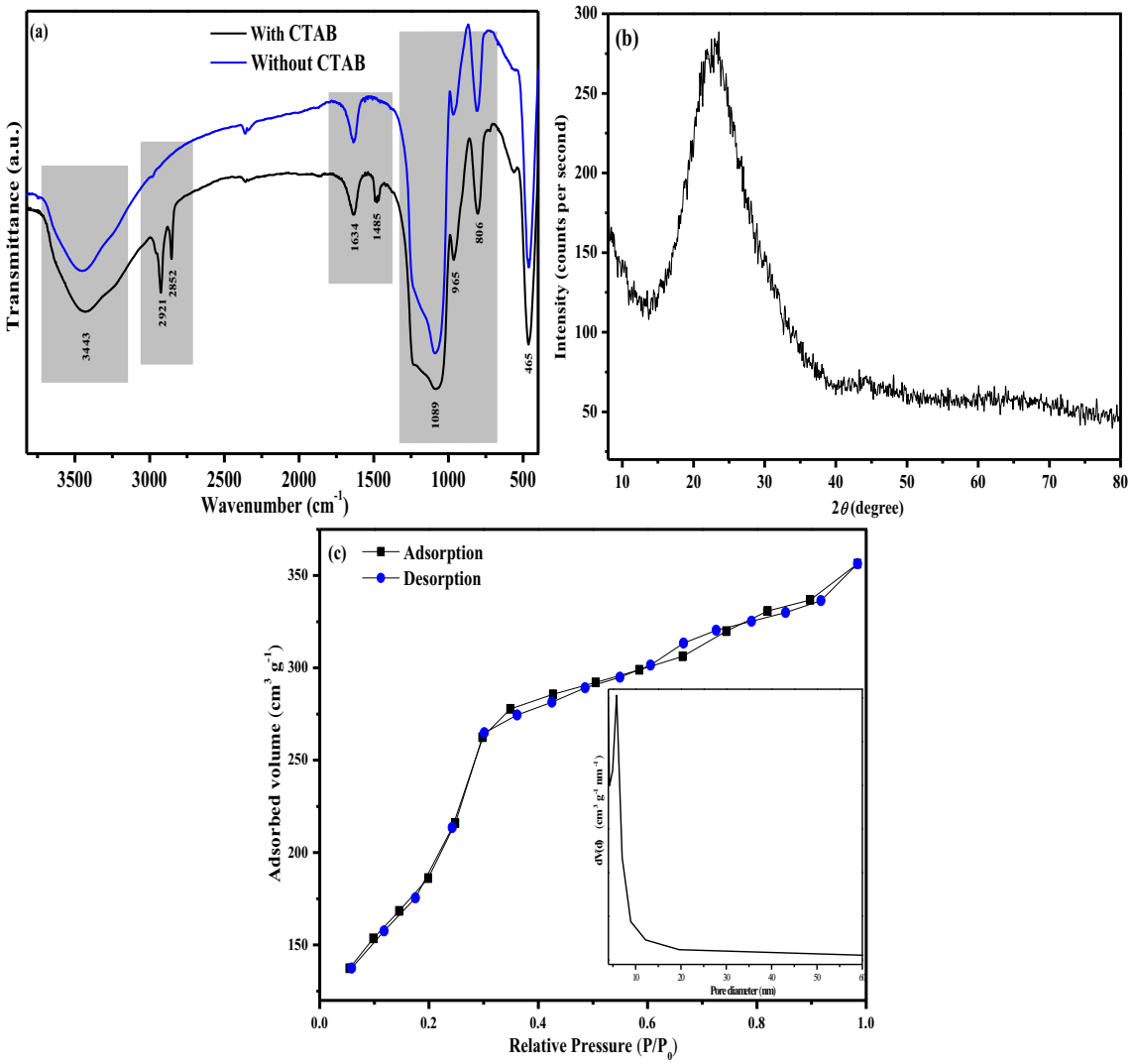

Fig. 1 FTIR spectra of MCM-48 (RHA) mesoporous array before and after CTAB removal (**a**), XRD profile (**b**), and N_2 adsorption/desorption isotherms and BJH pore size distribution of MCM-48 (RHA) mesoporous material without CTAB surfactant (**c**)

stretching mode of siloxane (Si–O–Si) group, 965 cm^{-1} due to symmetric stretching of Si–O bond of Si–OH group, 806 cm^{-1} related to the symmetric stretching mode of Si–O bond, and 465 cm^{-1} due to the bending vibration of Si–O–Si group (Endud and Wong 2007; Jang et al. 2009; Sharma et al. 2021).

Although the MCM-48 (RHA) mesoporous matrix presents a high degree of ordering from the small angle XRD analysis, it is typical that mesoporous materials also have an amorphous diffraction pattern, as seen from the high angle XRD analysis (Fig. 1b), which can be attributed to the amorphous condensed silica framework of MCM-48 (RHA) array from the silica source used in its hydrothermal synthesis (Costa et al. 2020c).

Figure 1c shows the results of the liquid N_2 adsorption/desorption analysis for MCM-48 (RHA). It is possible to observe that the N_2 adsorption/desorption isotherms present a characteristic profile of type IV isotherm and type H1 hysteresis with high adsorption of liquid N_2, according to the IUPAC classification for nanostructured materials of the M41S family of mesoporous materials, like the MCM-48 (Santos et al. 2019; Costa et al. 2020c, 2020d). Furthermore, these results are confirmed by the narrow mesopore distribution shown by MCM-48 (RHA), which is a characteristic profile of mesoporous matrixes with well-defined regular arrays of mesopores and high N_2 adsorption values. The textural and structural features of the MCM-48 (RHA) mesoporous array were calculated from the N_2 adsorption and desorption isotherms, which are summarized in Table 1. In summary, the MCM-48 (RHA) mesoporous material showed (i) high surface area (S_{BET}) value, calculated from BET method; (ii) high pore volume (V) and total pore volume (V_T) values; and (iii) average pore diameter and pore diameter (D_{BJH}) values between the range of mesoporous materials, which were defined between 2 and 50 nm. The high degree of ordering of the cubic mesoporous structure of MCM-48 has been demonstrated previously by our group (Santos et al. 2019) from the small angle XRD analysis, which the (211) and (220) diffraction planes of mesostructured are assigned as *Ia3d* space-group symmetry. The two peaks confirm the presence of a nanostructure formed by well-ordered arrays of interconnected cubic channels. Furthermore, the calculated lattice constant (a_0) was of the order of 12.5 nm, which is in agreement with the results of the textural and structural parameters presented in Table 1.

The SEM images obtained for untreated and treated RH and RHA, as well as for the MCM-48 (RHA) are shown in Fig. 2. The untreated RH showed an external epidermis, which is well-organized and has a rippled surface with an elongated and contorted shape, as well as the appearance of a corn cob. However, after the acid treatment carried out therein (Fig. 2ii), it is possible to observe that the surface of the RH has become more rough, due to the dilution or destruction of the amorphous region of the fibers present in the rice husk (Johara et al. 2012; Costa and Paranhos 2018). Thus, the external epidermis of the RHA presents the same characteristic of the raw RH; however, in the external epidermis, it concentrates the greater percentage of silica (Della et al. 2002, 2005). Therefore, Fig. 2iii shows the internal epidermis of the RHA, which shows the porous structure known as the silica skeleton, from the burning of the organic matter of the RH fibers, and this region also contains a considerable amount of silica (Liou 2004; Ahmed and Adam 2007).

The morphology of the MCM-48 (RHA) mesoporous material was evaluated by SEM, as shown in the image presented in Fig. 2iv. Thus, it is possible to observe that the MCM-48 (RHA) presented a morphology consisting of uniform spherical-like nanoparticles of high porosity from the framework amorphous of mesoporous architecture, which is a typical feature of the nanostructured mesoporous array of the M41S family (Costa et al. 2015; Saleh 2015). From the SEM-EDS analysis, it was possible to determine the chemical composition of the MCM-48 (RHA) (Fig. 3). The MCM-48 (RHA) presented high content of Si and O, as these are the main constituents of the framework of the amorphous material responsible for the formation of the MCM-48 (RHA) mesoporous material.

Multivariate optimization of adsorption procedure

Usually, the adsorption procedures are carried using a univariate methodology, which requires a high number of experiments, and consequently greater waste generation and higher cost. To get around these problems, a factorial design was used to optimize the variables involved in adsorption procedures. Table 2 shows a matrix experimental for the full factorial design (2^4) containing 19 experiments with real and coded values and the response in function of the % removal of Sb. Before evaluating the best conditions for the % removal of Sb, it was necessary to evaluate the quality of the linear model obtained from the factorial design. To check the quality of the linear model, an analysis of variance (ANOVA) was performed, and the results are available in Table 3.

Table 1 Textural and structural properties of MCM-48 (RHA) mesoporous material

Sample	S_{BET} (m^2 g^{-1})	V (cm^3 g^{-1})	V_T (cm^3 g^{-1})	D_{BJH} (nm)	Average pore diameter (nm)
MCM-48 (RHA)	820.9	0.2	0.6	3.7	2.7

S_{BET}, BET surface area; V, pore volume; V_T, total pore volume; D_{BJH}, pore diameter

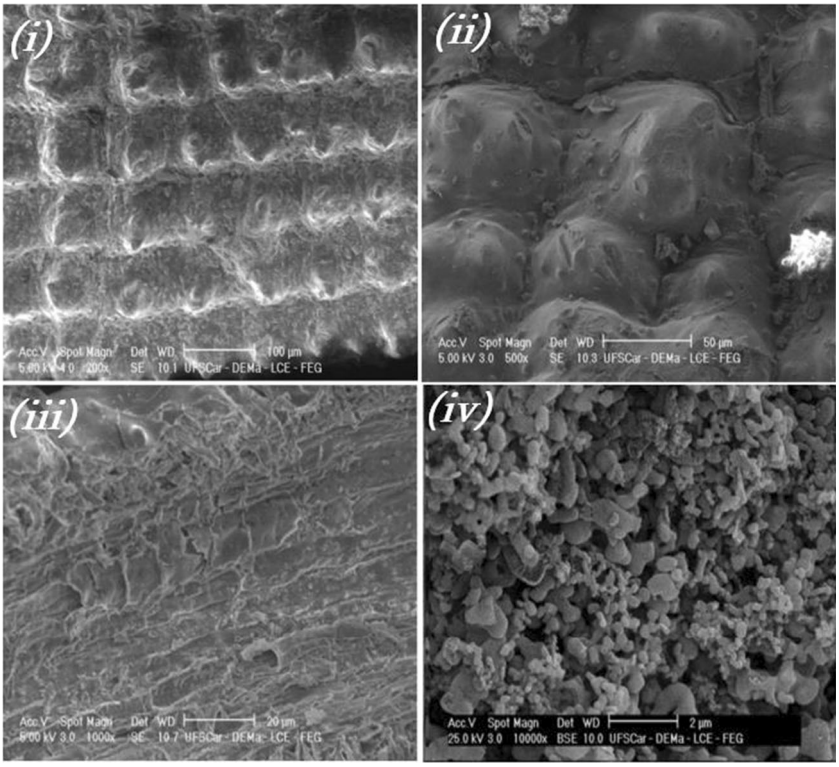

Fig. 2 MEV of untreated (**i**) and treated RH (**ii**), treated RHA (**iii**), and MCM-48 (RHA) mesoporous array (**iv**)

The first step for the evaluation of the model is checking the significance of regression. For that, a comparison between the ratio of mean square of regression (MS_R) and mean square of residue (MS_r) was performed. In this case, the $F_{calculated}$ (51.8) was 17-fold higher than the $F_{tabulated}$ (3.1) at the 95% confidence level. These data demonstrate that the regression of the model is highly significant, which gives credibility to the linear model. The second step for the evaluation of the model is checking if there is lack of fit. In this case, a comparison between the ratio of mean square of lack of fit (MS_{lof}) and mean square of pure error (MS_{pe}) was performed. It was observed that the model does not present lack of fit because the $F_{calculated}$ (6.2) was lower than the value of $F_{tabulated}$ (19.0) at the 95% confidence level. In addition, the quality of the linear model also was evaluated by analyzing the graphic of predicted values versus observed, as shown in Fig. 4a. Thus, it is possible to observe that the model is well adjusted with a 99% regression percentage. This observation confirms the good fit of the model that is verified in Table 3.

After data processing, the evaluation of best conditions for adsorption procedure for the % Sb removal was performed by analysis of Pareto graph (Fig. 4b), evaluating the significance of the variables and their interactions, at a confidence level of 95% (Ferreira et al. 2018). According to the results presented in Fig. 4b (Pareto graph), the first-order variables are all significant. In addition, some second- and third-order interactions are also significant. The discussion of the influence of variables on the % Sb removal will follow the order of significance presented in the Pareto graph, according to the following sequence: (i) adsorbent mass, (ii) adsorption time, (iii) solution pH, and (iv) concentration of the Sb standard.

The adsorbent mass is the most important variable, and the adsorption efficiency increases with the increase in the mass of the MCM-48 (RHA) adsorbent material. Removal efficiency of Sb can be related to the increased surface area of mesoporous array, as well as the availability of more adsorption sites for Sb within the framework of the architectured matrix of MCM-48 (RHA) (Costa and Paranhos 2020; Costa et al. 2020b). Thus, to ensure a high removal percentage of Sb, we choose to use a mass of 45 mg.

The adsorption time is an important variable, especially when new adsorbents are tested (Costa and Paranhos 2019; Costa et al. 2020a, 2020d). In this study, the adsorption time showed a positive effect on the removal efficiency of Sb by MCM-48 (RHA) adsorbent. From the analysis of Table 2, it is possible to observe that the evaluated adsorption times presented excellent results, especially when combined with the condition of greater mass of adsorbent was used. This behavior can be seen between experiments 9 and 19, as shown in Table 2, from which we can highlight experiments 9 and 10, where there was fast adsorption at a low concentration of Sb in the initial 5 min of contact between the adsorbent material and adsorbate, whose removal values were 80 and 84%, respectively. This fast adsorption is due to the interaction of Sb with the most external local sites on the surface of MCM-48 (RHA) (Costa et al. 2014, 2015). Figure 4b also shows that the

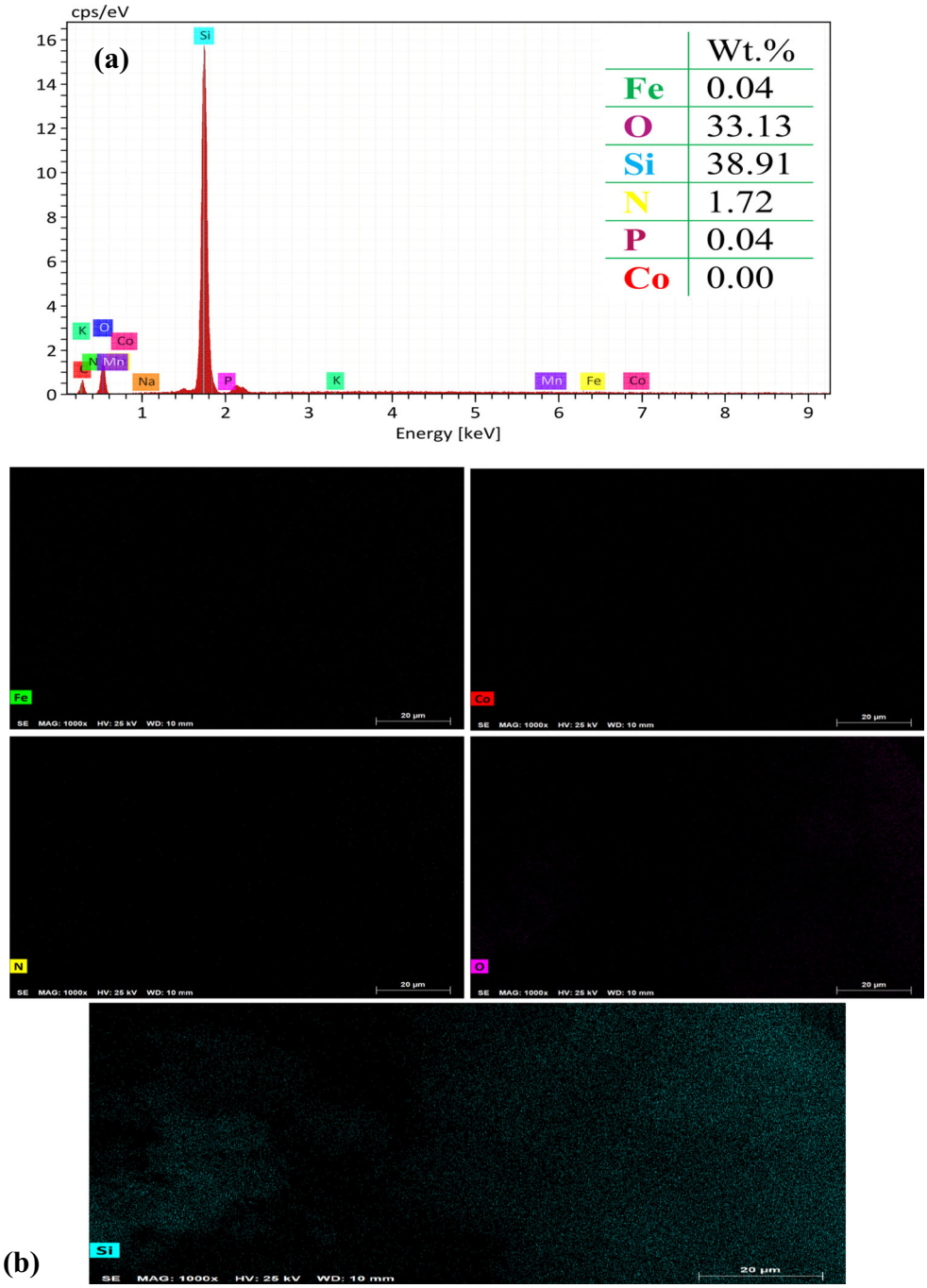

Fig. 3 EDS spectrograph (**a**) and elemental mapping (**b**) of MCM-48 (RHA) mesoporous material

interaction between adsorbent mass and adsorption time is significant with a negative effect, that is, one of the variables must be tested at the maximum level and the other at the lower level. As the adsorbent mass has been fixed at the maximum level (45 mg), the adsorption time can be fixed using the condition of the central point (60 min).

The solution pH is an important factor affecting the removal of the metal species in aqueous solution. The dependence on metal adsorption in function of the solution pH is related to the type of metal that is in the solution, and to the state of ionization of the adsorbent functional group, which affects the availability of the binding sites. Under the established conditions, the experiments were carried at solution pH ranging from 2 to 10, as shown in Table 2. It is possible to observe in Table 2 that the removal percentage was adequate in the pH range evaluated, except in experiments 1, 2, 3, 5, 6, and 7, which showed removal efficiency below 80%. However, it is possible to verify that in the mentioned experiments, the adsorbent mass tested was 5 mg, which seems to interfere in the Sb removal in function of the tested pH range. In the

Table 2 Matrix of the full factorial design (2^4) with real and coded values and the response in function of the % removal of Sb

Experiment	Variables				% Sb removal
	pH	Adsorption time (min)	Concentration of Sb standard (mol L^{-1})	Adsorbent mass (mg)	
1	2 (−1)	5 (−1)	2 (−1)	5 (−1)	24
2	10 (1)	5 (−1)	2 (−1)	5 (−1)	60
3	2 (−1)	115 (1)	2 (−1)	5 (−1)	74
4	10 (1)	115 (1)	2 (−1)	5 (−1)	85
5	2 (−1)	5 (−1)	8 (1)	5 (−1)	55
6	10 (1)	5 (−1)	8 (1)	5 (−1)	76
7	2 (−1)	115 (1)	8 (1)	5 (−1)	74
8	10 (1)	115 (1)	8 (1)	5 (−1)	82
9	2 (−1)	5 (−1)	2 (−1)	45 (1)	80
10	10 (1)	5 (−1)	2 (−1)	45 (1)	84
11	2 (−1)	115 (1)	2 (−1)	45 (1)	89
12	10 (1)	115 (1)	2 (−1)	45 (1)	89
13	2 (−1)	5 (−1)	8 (1)	45 (1)	92
14	10 (1)	5 (−1)	8 (1)	45 (1)	94
15	2 (−1)	115 (1)	8 (1)	45 (1)	95
16	10 (1)	115 (1)	8 (1)	45 (1)	94
17 (*CP*)	6 (0)	60 (0)	5 (0)	25 (0)	93
18 (*CP*)	6 (0)	60 (0)	5 (0)	25 (0)	93
19 (*CP*)	6 (0)	60 (0)	5 (0)	25 (0)	93

CP, central point

experiments that used mass of 25 and 45 mg, the removal percentage stayed above 80%, reaching a maximum efficiency of 95% (experiment 15) at pH 2. The excellent removal efficiency of Sb by the MCM-48 (RHA) at pH 2 is due to the protonation of the silanol and siloxane groups on the surface of mesoporous architecture, thus causing a good electrostatic interaction between the protonated groups of the adsorbent material with the metallic species of Sb (Costa and Paranhos 2019; Costa et al. 2019b, 2020a). On the other hand, the results obtained showed that the studied material has a good adsorption capacity in the Sb remediation in solution pH values ranging between 2 and 10 using a mass greater than 25 mg. As the purpose of applying MCM-48-based mesoporous array is to remove Sb from different water samples, we understand that there is no need to establish an optimal pH condition. In this case, we can establish a pH range between 2 and 10 using an adsorbent mass of 45 mg. The no need for pH adjustment is interesting and increases the frequency of the analytical method proposed.

In this study, it is also possible to observe that the mesoporous material presents an excellent removal at different Sb concentration values, mainly in experiments 4, 11–12, 14–15, and 17–19. This behavior is very interesting because it shows the versatility of the adsorbent material against different pollutant concentration values and a wide range of residual solution pH. Figure 5 shows the graph of the desirability to the variables evaluated with the most appropriate condition marked with a red line. Thus, the established conditions were as follows: adsorbent mass: 45 mg; adsorption time: 60 min; pH: ranged from 2 to 10; concentration of the Sb standard: 8 mol L^{-1}. Finally, Table 4 presents a comparison of the removal efficiency of Sb by MCM-48 (RHA) with some adsorbent materials presented in the literature. It is possible to observe that the MCM-48 (RHA) presented a removal percentage as good as the values found for adsorbent materials NaY@C (Yan et al. 2020), TNS (Liu et al. 2021), black soil (Fan et al. 2020, 2021), NMSH (Deng et al. 2020), Fe-MIL-88B (Cheng et al. 2020), Bentonite (Xi et al. 2011), and Silica (Fan et al. 2016).

Application using real samples

The proposed method of adsorption was applied for the Sb removal in samples of environmental interest, in the case of this study in water samples. Commonly, the concentration of Sb in water samples is at a trace level (ppb), in this sense the samples analyzed were enriched with known concentrations of Sb. A total of five samples were analyzed and Sb concentrations (~8 ppm) were added. These samples were submitted to the adsorption procedure with the optimized conditions,

Table 3 ANOVA table in function of the % removal of Sb with a 95% confidence level

Parameters	*SS*	*d.f*	*MS*	$F_{calculated}$	$F_{tabulated}$
Regression	5102.0	4	1275.0	51.8	3.1
Residual	57.3	14	4.1		
Lack of fit	49.3	2	24.6	6.2	19.0
Pure error	8.0	2	4.0		
Total	5159.3	18			

SS, sum of square; *d.f*, degree of freedom; *MS*, mean of square

and subsequently, the final aqueous solution was subjected to analysis by ICP OES. From Eq. 1, it was possible to calculate the % removal of Sb which varied from 88 to 96%. The adsorbent proposed had no matrix effect in the adsorption process, and thus confirming that it can be used in the remediation of Sb in water samples.

Conclusions

In this present approach, we carry out the synthesis of MCM-48-based mesoporous array via an inexpensive, sustainable, and eco-friendly hydrothermal method using an alternative silica source extracted from the rice husk ash, which was posteriorly tested as an adsorbent material for the Sb remediation. The prepared MCM-48 (RHA) array exhibited an amorphous framework with the N_2 adsorption/desorption isotherms of type IV and type H1 hysteresis, due to the high N_2 adsorption of three-dimensional cubic mesostructure with *Ia3d* space-group symmetry, whose S_{BET}, V_T, and D_{BJH} values obtained

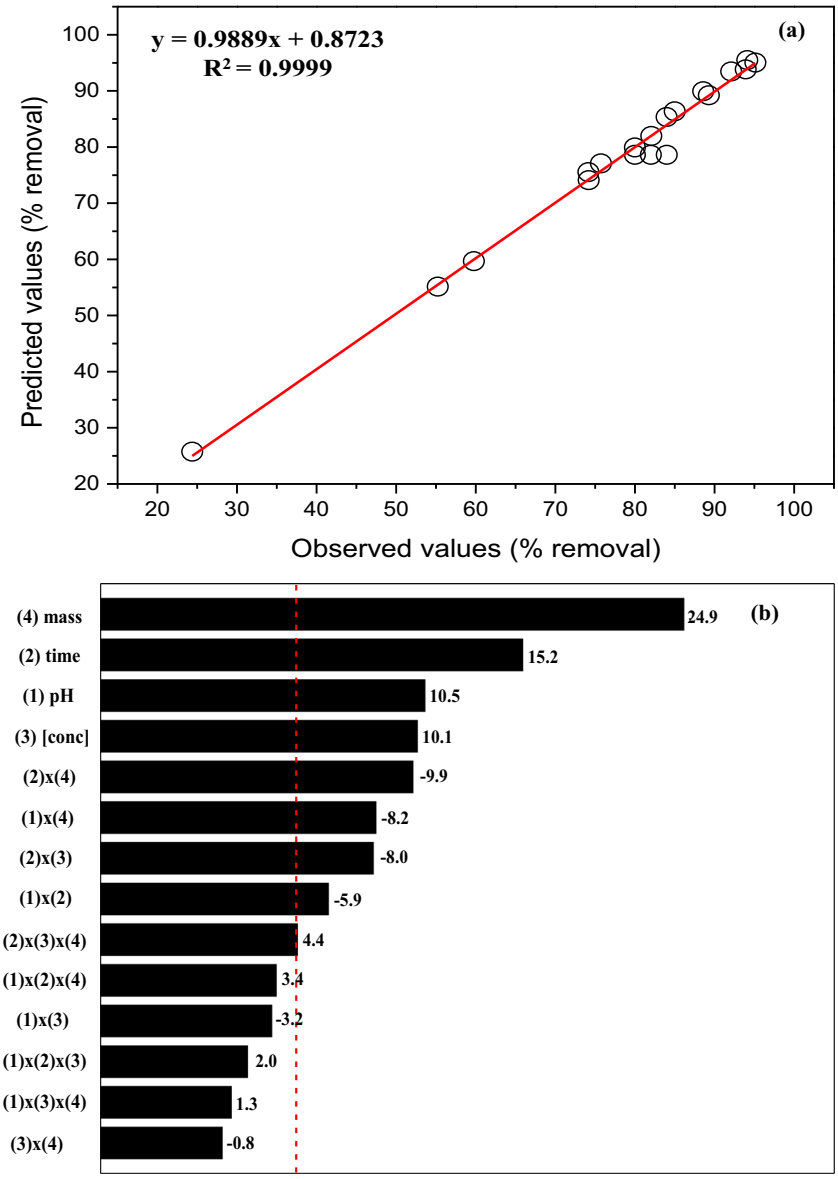

Fig. 4 Observed values versus predicted values, for linear model in function of the % Sb removal (**a**) and Pareto graph of effects for full factorial design, in function of the % Sb removal (**b**)

Table 4 Comparison of removal efficiency

Adsorbent	Optimum pH	Equilibrium time	Sb state	Removal efficiency (%)	Reference
NaY@Ce[a]	7	720 min	Sb(III) Sb(V)	78 74	(Yan et al. 2020)
TNS[b]	2	30 min	Sb(III)	90	(Liu et al. 2021)
Black soil[c]	3	720 min	Sb(V)	80	(Fan et al. 2021)
Black soil	4	35 h	Sb(V)	81	(Fan et al. 2020)
NMSH[d]	7	4 h	Sb(V)	99	(Deng et al. 2020)
Fe-MIL-88B[e]	6	-	Sb(III) Sb(V)	>90	(Cheng et al. 2020)
Bentonite[f]	6	~24 h	Sb(III) Sb(V)	90 80	(Xi et al. 2011)
Silica[g]	3–9	20 min	Sb(III)	>90	(Fan et al. 2016)
MCM-48 (RHA)[h]	2	115 min	Total Sb	95	Present study

[a] Cerium hydroxide loaded Y-tape molecular sieve

[b] Titanate nanosheets

[c] Black soil sample

[d] Amino-functionalized hydrothermal biochar modified with nitric acid and nicotinamide

[e] Iron-based metal-organic framework

[f] Silicate clay mineral

[g] Mercapto-functionalized silica-supported organic-inorganic hybrid

[h] Mobil Composition of Matter No. 48

were in the order of 820.9 m^2 g^{-1}, 0.6 cm^3 g^{-1}, and 3.7 nm, respectively. In addition, the mesoporous matrix presents a narrow mesopores distribution and uniform spherical particles, typical of the architectures with well-defined regular

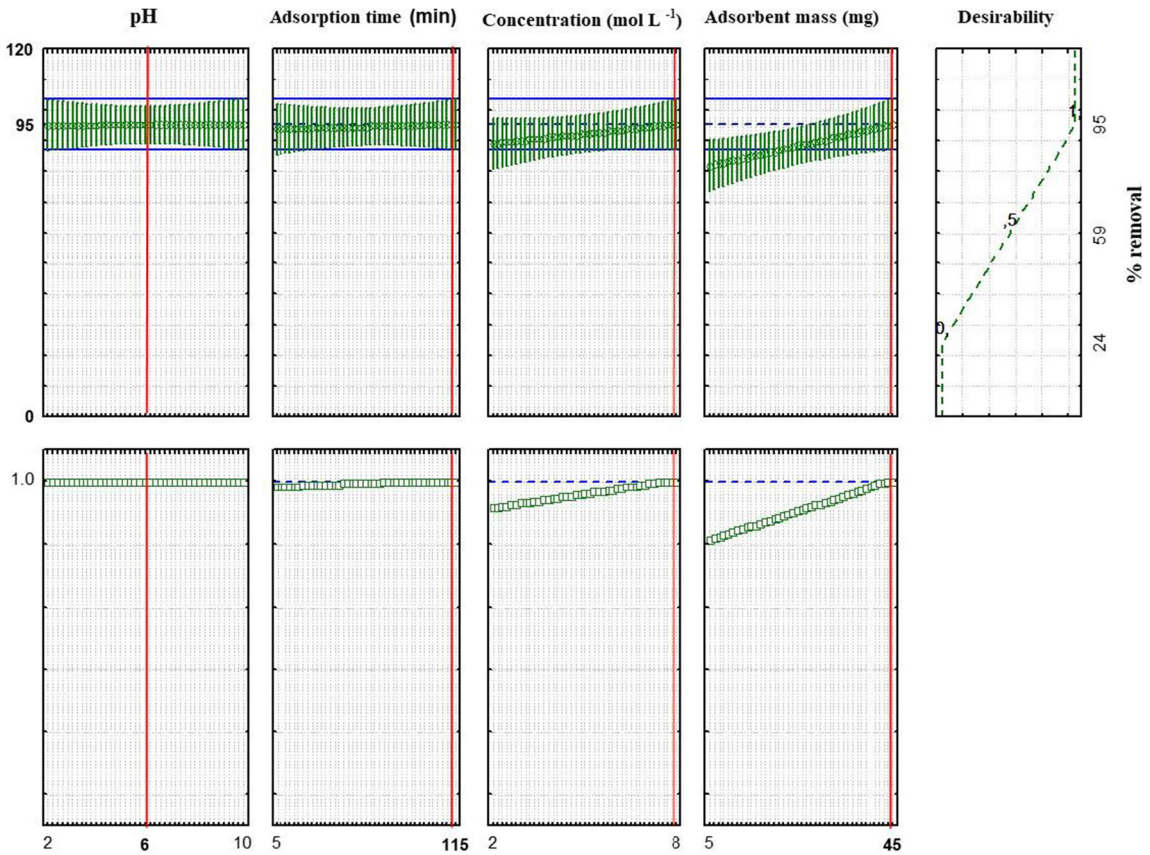

Fig. 5 Graphic of profiles of predicted values and desirability in function of the % Sb removal

channels. Thus, these advanced structural and textural features significantly influenced the remediation capacity of eco-friendly MCM-48 (RHA) to adsorb Sb in an aqueous medium.

The variables of the adsorption procedure of Sb, which were optimized through a full factorial design (2^4), proved the versatility of mesoporous array as an adsorbent metallic species. The factorial design was useful to find the optimized conditions using a smaller number of experiments, briefly (i) the MCM-48 (RHA) exhibited a fast and high adsorption efficiency at a low concentration of Sb, mainly in the initial 5 min of adsorption (experiments 9 and 10); (ii) the Pareto graph showed the following decreasing order of significance for Sb adsorption by MCM-48 (RHA): adsorbent mass > sorption time > solution pH > Sb standard concentration; (iii) finally, a maximum Sb removal efficiency of 95% was achieved at an equilibrium time of 115 min (pH 2) using 45 mg of MCM-48 (RHA) at an initial Sb concentration of 2 mol L^{-1}. On the other side, the MCM-48 (RHA) proved to be versatile for use as an adsorbent in the most different ranges of concentration and solution pH.

Author contribution José Arnaldo Santana Costa: conceptualization, methodology, validation, investigation, formal analysis, resources, writing—original draft. Vinicius Câmara Costa: conceptualization, methodology, validation, investigation, formal analysis, resources, writing—original draft. Matheus Lima de Mello: methodology, validation, formal analysis. Caio Marcio Paranhos: conceptualization, methodology, validation, investigation, formal analysis, resources, writing—original draft, supervision

Funding This study received financial support from Fundação de Amparo à Pesquisa do Estado de São Paulo (FAPESP) (Grants 2017/06775-5 and 2021/01187-3) and Centro de Desenvolvimento de Materiais Funcionais (CDMF) (Grant 2013/07296-2).

Availability of data and materials The authors declare that data supporting the findings of this study are available within the article.

Declarations

Ethics approval Not applicable.

Consent to participate Not applicable.

Consent for publication The authors transfer to Springer the publication rights.

Competing interests The authors declare no competing interests.

References

Adio SO, Omar MH, Asif M, Saleh TA (2017) Arsenic and selenium removal from water using biosynthesized nanoscale zero-valent iron: a factorial design analysis. Process Saf Environ Prot 107:518–527. https://doi.org/10.1016/j.psep.2017.03.004

Ahmed AE, Adam F (2007) Indium incorporated silica from rice husk and its catalytic activity. Microporous Mesoporous Mater 103:284–295. https://doi.org/10.1016/j.micromeso.2007.01.055

Akhil D, Lakshmi D, Senthil Kumar P, Vo DVN, Kartik A (2021) Occurrence and removal of antibiotics from industrial wastewater. Environ Chem Lett 19:1477–1507. https://doi.org/10.1007/s10311-020-01152-0

Ambursa MM, Sudarsanam P, Voon LH, Hamid SBA, Bhargava SK (2017) Bimetallic Cu-Ni catalysts supported on MCM-41 and Ti-MCM-41 porous materials for hydrodeoxygenation of lignin model compound into transportation fuels. Fuel Process Technol 162:87–97. https://doi.org/10.1016/J.FUPROC.2017.03.008

Antoniadis V, Golia EE, Liu Y-T, Wang SL, Shaheen SM, Rinklebe J (2019) Soil and maize contamination by trace elements and associated health risk assessment in the industrial area of Volos, Greece. Environ Int 124:79–88. https://doi.org/10.1016/j.envint.2018.12.053

Aquino FWB, Paranhos CM, Pereira-Filho ER (2016) Method for the production of acrylonitrile–butadiene–styrene (ABS) and polycarbonate (PC)/ABS standards for direct Sb determination in plastics from e-waste using laser-induced breakdown spectroscopy. J Anal At Spectrom 31:1228–1233. https://doi.org/10.1039/C6JA00038J

Arumugam A, Karuppasamy G, Jegadeesan GB (2018) Synthesis of mesoporous materials from bamboo leaf ash and catalytic properties of immobilized lipase for hydrolysis of rubber seed oil. Mater Lett 225:113–116. https://doi.org/10.1016/J.MATLET.2018.04.122

Castillo X, Pizarro J, Ortiz C, Cid H, Flores M, de Canck E, van der Voort P (2018) A cheap mesoporous silica from fly ash as an outstanding adsorbent for sulfate in water. Microporous Mesoporous Mater 272:184–192. https://doi.org/10.1016/J.MICROMESO.2018.06.014

Chen Z, Zhang S, Liu Y, Alharbi NS, Rabah SO, Wang S, Wang X (2020) Synthesis and fabrication of g-C3N4-based materials and their application in elimination of pollutants. Sci Total Environ 731:139054. https://doi.org/10.1016/j.scitotenv.2020.139054

Cheng K, nan WY, Zhang B, Li F (2020) New insights into the removal of antimony from water using an iron-based metal-organic framework: adsorption behaviors and mechanisms. Colloids Surfaces A Physicochem Eng Asp 602:125054. https://doi.org/10.1016/j.colsurfa.2020.125054

Chu J, Mao J, He M (2019) Anthropogenic antimony flow analysis and evaluation in China. Sci Total Environ 683:659–667. https://doi.org/10.1016/j.scitotenv.2019.05.293

Costa JAS, Paranhos CM (2018) Systematic evaluation of amorphous silica production from rice husk ashes. J Clean Prod 192:688–697. https://doi.org/10.1016/j.jclepro.2018.05.028

Costa JAS, Paranhos CM (2019) Evaluation of rice husk ash in adsorption of Remazol Red dye from aqueous media. SN Appl Sci 1:397. https://doi.org/10.1007/s42452-019-0436-1

Costa JAS, Paranhos CM (2020) Mitigation of silica-rich wastes: an alternative to the synthesis eco-friendly silica-based mesoporous materials. Microporous Mesoporous Mater 309:110570. https://doi.org/10.1016/j.micromeso.2020.110570

Costa JAS, Garcia ACFS, Santos DO et al (2014) A new functionalized MCM-41 mesoporous material for use in environmental applications. J Braz Chem Soc 25:197–207. https://doi.org/10.5935/0103-5053.20130284

Costa JAS, Garcia ACFS, Santos DO, Sarmento VHV, de Mesquita ME, Romão LPC (2015) Applications of inorganic-organic mesoporous materials constructed by self-assembly processes for removal of benzo[k]fluoranthene and benzo[b]fluoranthene. J Sol-Gel Sci Technol 75:495–507. https://doi.org/10.1007/s10971-015-3720-6

Costa JAS, de Jesus RA, da Silva CMP, Romão LPC (2017a) Efficient adsorption of a mixture of polycyclic aromatic hydrocarbons (PAHs) by Si–MCM–41 mesoporous molecular sieve. Powder Technol 308:434–441. https://doi.org/10.1016/j.powtec.2016.12.035

Costa JAS, de Jesus RA, Dorst DD, Pinatti IM, Oliveira LMR, de Mesquita ME, Paranhos CM (2017b) Photoluminescent properties of the europium and terbium complexes covalently bonded to functionalized mesoporous material PABA-MCM-41. J Lumin 192: 1149–1156. https://doi.org/10.1016/j.jlumin.2017.08.046

Costa VC, de Babos DV, de Aquino FWB, Virgílio A, Amorim FAC, Pereira-Filho ER (2018) Direct determination of Ca, K and Mg in cassava flour samples by laser-induced breakdown spectroscopy (LIBS). Food Anal Methods 11:1886–1896. https://doi.org/10.1007/s12161-017-1086-9

Costa JAS, Sarmento VHV, Romão LPC, Paranhos CM (2019a) Adsorption of organic compounds on mesoporous material from rice husk ash (RHA). Biomass Convers Biorefinery. 10:1105–1120. https://doi.org/10.1007/s13399-019-00476-4

Costa JAS, Sarmento VHV, Romão LPC, Paranhos CM (2019b) Synthesis of functionalized mesoporous material from rice husk ash and its application in the removal of the polycyclic aromatic hydrocarbons. Environ Sci Pollut Res 26:25476–25490. https://doi.org/10.1007/s11356-019-05852-1

Costa VC, Pinheiro FC, Amorim FAC, Paranhos da Silva EG, Pereira-Filho ER (2019c) Multivariate optimization for the development of a sample preparation procedure and evaluation of calibration strategies for nutrient elements determination in handmade chocolate. Microchem J 150:104166. https://doi.org/10.1016/j.microc.2019.104166

Costa JAS, Costa VC, Pereira-Filho ER, Paranhos CM (2020a) Removal of Cr(VI) from wastewater of the tannery industry by functionalized mesoporous material. Silicon 12:1895–1903. https://doi.org/10.1007/s12633-019-00315-1

Costa JAS, de Jesus RA, Santos DO, Mano JF, Romão LPC, Paranhos CM (2020b) Recent progresses in the adsorption of organic, inorganic, and gas compounds by MCM-41-based mesoporous materials. Microporous Mesoporous Mater 291:109698. https://doi.org/10.1016/j.micromeso.2019.109698

Costa JAS, Sarmento VHV, Romão LPC, Paranhos CM (2020c) Removal of polycyclic aromatic hydrocarbons from aqueous media with polysulfone/MCM-41 mixed matrix membranes. J Memb Sci 601:117912. https://doi.org/10.1016/j.memsci.2020.117912

Costa JAS, Sarmento VHV, Romão LPC, Paranhos CM (2020d) Performance of the MCM-41-NH2 functionalized mesoporous material synthetized from the rice husk ash on the removal of the polycyclic aromatic hydrocarbons. Silicon 12:1913–1923. https://doi.org/10.1007/s12633-019-00289-0

Costa JAS, Vedovello P, Paranhos CM (2020e) Use of Ionic liquid as template for hydrothermal synthesis of the MCM-41 mesoporous material. Silicon 12:289–294. https://doi.org/10.1007/s12633-019-00121-9

Costa JAS, de Jesus RA, Santos DO, Neris JB, Figueiredo RT, Paranhos CM (2021a) Synthesis, functionalization, and environmental application of silica-based mesoporous materials of the M41S and SBA-n families: a review. J Environ Chem Eng 9:105259. https://doi.org/10.1016/j.jece.2021.105259

Costa JAS, Sarmento VHV, Romão LPC, Paranhos CM (2021b) Polycyclic aromatic hydrocarbons removal from aqueous solution with PABA-MCM-41/polyethersulfone mixed matrix membranes. Silicon. https://doi.org/10.1007/s12633-021-01165-6

de Jesus RA, de Assis GC, de Oliveira RJ, Costa JAS, da Silva CMP, Bilal M, Iqbal HMN, Ferreira LFR, Figueiredo RT (2021) Environmental remediation potentialities of metal and metal oxide nanoparticles: mechanistic biosynthesis, influencing factors, and application standpoint. Environ Technol Innov 24:101851. https://doi.org/10.1016/j.eti.2021.101851

de Sá IP, Higuera JM, Costa VC, Costa JAS, da Silva CMP, Nogueira ARA (2020) Determination of trace elements in meat and fish samples by MIP OES using solid-phase extraction. Food Anal Methods 13:238–248. https://doi.org/10.1007/s12161-019-01615-3

Della V, Kuhn I, Hotza D (2002) Rice husk ash as an elemente source for active silicaproduction. Mater Lett 57:818–821. https://doi.org/10.1016/S0167-577X(02)00879-0

Della VP, Kühn I, Hotza D (2005) Reciclagem de Resíduos Agro-Industriais: Cinza de Casca de Arroz como Fonte Alternativa de Sílica. Cerâmica Ind 10:22–25

Deng J, Li X, Wei X, Liu Y, Liang J, Shao Y, Huang W, Cheng X (2020) Different adsorption behaviors and mechanisms of a novel amino-functionalized hydrothermal biochar for hexavalent chromium and pentavalent antimony. Bioresour Technol 310:123438. https://doi.org/10.1016/j.biortech.2020.123438

Doustkhah E, Lin J, Rostamnia S, Len C, Luque R, Luo X, Bando Y, Wu KCW, Kim J, Yamauchi Y, Ide Y (2019) Development of Sulfonic-acid-functionalized mesoporous materials: synthesis and catalytic applications. Chem A Eur J 25:1614–1635. https://doi.org/10.1002/chem.201802183

Endud S, Wong KL (2007) Mesoporous silica MCM-48 molecular sieve modified with SnCl2in alkaline medium for selective oxidation of alcohol. Microporous Mesoporous Mater 101:256–263. https://doi.org/10.1016/j.micromeso.2006.12.029

Fan HT, Sun W, Jiang B, Wang QJ, Li DW, Huang CC, Wang KJ, Zhang ZG, Li WX (2016) Adsorption of antimony(III) from aqueous solution by mercapto-functionalized silica-supported organic-inorganic hybrid sorbent: mechanism insights. Chem Eng J 286:128–138. https://doi.org/10.1016/j.cej.2015.10.048

Fan Y, Zheng C, Liu H, He C, Shen Z, Zhang TC (2020) Effect of pH on the adsorption of arsenic(V) and antimony(V) by the black soil in three systems: performance and mechanism. Ecotoxicol Environ Saf 191:110145. https://doi.org/10.1016/j.ecoenv.2019.110145

Fan Y, Zheng C, Lin Z, Huo A, Li R, He C (2021) Influence of sulfamethazine (SMT) on the adsorption of antimony by the black soil: implication for the complexation between SMT and antimony. Sci Total Environ 760:143318. https://doi.org/10.1016/j.scitotenv.2020.143318

Ferreira SLC, Caires AO, Borges T da S, et al. (2017) Robustness evaluation in analytical methods optimized using experimental designs. Microchem J 131:163–169. https://doi.org/10.1016/j.microc.2016.12.004

Ferreira SLC, Lemos VA, de Carvalho VS, da Silva EGP, Queiroz AFS, Felix CSA, da Silva DLF, Dourado GB, Oliveira RV (2018) Multivariate optimization techniques in analytical chemistry - an overview. Microchem J 140:176–182. https://doi.org/10.1016/j.microc.2018.04.002

Fitaroni LB, Venâncio T, Tanaka FH, Gimenez JCF, Costa JAS, Cruz SA (2019) Organically modified sepiolite: thermal treatment and chemical and morphological properties. Appl Clay Sci 179:105149. https://doi.org/10.1016/j.clay.2019.105149

Gamela RR, Costa VC, Pereira-Filho ER (2020) Multivariate Optimization of ultrasound-assisted extraction procedure for the determination of Ca, Fe, K, Mg, Mn, P, and Zn in pepper samples by ICP OES. Food Anal Methods 13:69–77. https://doi.org/10.1007/s12161-019-01524-5

Ghorbani F, Younesi H, Mehraban Z et al (2013) Preparation and characterization of highly pure silica from sedge as agricultural waste and its utilization in the synthesis of mesoporous silica MCM-41. J Taiwan Inst Chem Eng 44:821–828. https://doi.org/10.1016/j.jtice.2013.01.019

Jang HT, Park YK, Ko YS, Lee JY, Margandan B (2009) Highly siliceous MCM-48 from rice husk ash for CO2 adsorption. Int J Greenh Gas Control 3:545–549. https://doi.org/10.1016/j.ijggc.2009.02.008

Johara N, Ahmada I, Dufresne A (2012) Extraction, preparation and characterization of cellulose fibres and nanocrystals from rice husk. Ind Crops Prod 37:93–99. https://doi.org/10.1016/j.indcrop.2011.12.016

Kankala RK, Han Y, Na J et al (2020) Nanoarchitectured structure and surface biofunctionality of mesoporous silica nanoparticles. Adv Mater 32:1907035. https://doi.org/10.1002/adma.201907035

Li X, Dong L, Zhang J, Hu C, Zhang X, Cai Y, Shao S (2019) In-situ catalytic upgrading of biomass-derived vapors using HZSM-5 and MCM-41: effects of mixing ratios on bio-oil preparation. J Energy Inst 92:136–143. https://doi.org/10.1016/J.JOEI.2017.10.015

Liou TH (2004) Preparation and characterization of nano-structured silica from rice husk. Mater Sci Eng A 364:313–323. https://doi.org/10.1016/j.msea.2003.08.045

Liu C, Li Y, Wang X, Li B, Zhou Y, Liu D, Liu D, Liu S (2021) Efficient extraction of antimony(III) by titanate nanosheets: study on adsorption behavior and mechanism. Ecotoxicol Environ Saf 207:111271. https://doi.org/10.1016/j.ecoenv.2020.111271

Ma Y, Chen H, Shi Y, Yuan S (2016) Low cost synthesis of mesoporous molecular sieve MCM-41 from wheat straw ash using CTAB as surfactant. Mater Res Bull 77:258–264. https://doi.org/10.1016/J.MATERRESBULL.2016.01.052

Meng L, Wu M, Chen H, Xi Y, Huang M, Luo X (2020) Rejection of antimony in dyeing and printing wastewater by forward osmosis. Sci Total Environ 745:141015. https://doi.org/10.1016/j.scitotenv.2020.141015

Norsuraya S, Fazlena H, Norhasyimi R (2016) Sugarcane bagasse as a renewable source of silica to synthesize Santa Barbara Amorphous-15 (SBA-15). Procedia Eng 148:839–846. https://doi.org/10.1016/J.PROENG.2016.06.627

Saleh TA (2015) Isotherm, kinetic, and thermodynamic studies on Hg(II) adsorption from aqueous solution by silica- multiwall carbon nanotubes. Environ Sci Pollut Res 22:16721–16731. https://doi.org/10.1007/s11356-015-4866-z

Saleh TA (2018) Simultaneous adsorptive desulfurization of diesel fuel over bimetallic nanoparticles loaded on activated carbon. J Clean Prod 172:2123–2132. https://doi.org/10.1016/j.jclepro.2017.11.208

Saleh TA (2020) Trends in the sample preparation and analysis of nanomaterials as environmental contaminants. Trends Environ7. Anal Chem 28:e00101. https://doi.org/10.1016/j.teac.2020.e00101

Saleh TA, Sarı A, Tuzen M (2017) Optimization of parameters with experimental design for the adsorption of mercury using polyethylenimine modified-activated carbon. J Environ Chem Eng 5:1079–1088. https://doi.org/10.1016/j.jece.2017.01.032

Saleh TA, Tuzen M, Sarı A (2018) Polyamide magnetic palygorskite for the simultaneous removal of Hg(II) and methyl mercury; with factorial design analysis. J Environ Manage 211:323–333. https://doi.org/10.1016/j.jenvman.2018.01.050

Santos LFS, de Jesus RA, Costa JAS, Gouveia LGT, de Mesquita ME, Navickiene S (2019) Evaluation of MCM-41 and MCM-48 mesoporous materials as sorbents in matrix solid phase dispersion method for the determination of pesticides in soursop fruit (Annona muricata). Inorg Chem Commun 101:45–51. https://doi.org/10.1016/j.inoche.2019.01.013

Sharma S, Singh UP, Singh AP (2021) Synthesis of MCM-41 supported cobalt (II) complex for the formation of polyhydroquinoline derivatives. Polyhedron 199:115102. https://doi.org/10.1016/j.poly.2021.115102

Sohrabnezhad S, Daraie Mooshangaie S (2019) In situ fabrication of n-type Ag/AgBr nanoparticles in MCM-41 with rice husk (RH/MCM-41) composite for the removal of Eriochrome Black-T. Mater Sci Eng B 240:16–22. https://doi.org/10.1016/J.MSEB.2019.01.007

Viczek SA, Aldrian A, Pomberger R, Sarc R (2020) Origins and carriers of Sb, As, Cd, Cl, Cr, Co, Pb, Hg, and Ni in mixed solid waste – a literature-based evaluation. Waste Manag 103:87–112. https://doi.org/10.1016/j.wasman.2019.12.009

Wang J, Xu Y, Ding B, Chang Z, Zhang X, Yamauchi Y, Wu KCW (2018) Confined self-assembly in two-dimensional interlayer space: monolayered mesoporous carbon nanosheets with in-plane orderly arranged mesopores and a highly graphitized framework. Angew Chemie Int Ed 57:2894–2898. https://doi.org/10.1002/anie.201712959

Xi J, He M, Lin C (2011) Adsorption of antimony(III) and antimony(V) on bentonite: kinetics, thermodynamics and anion competition. Microchem J 97:85–91. https://doi.org/10.1016/j.microc.2010.05.017

Xiang-Xue W, Xing L, Jia-Qi W, Hong-Tao Z (2019) Recent advances in carbon nitride-based nanomaterials for the removal of heavy metal ions from aqueous solution. J Inorg Mater 436. https://doi.org/10.15541/jim20190436

Xu D, Gao B, Peng W, Gao L, Li Y (2019) Geochemical and health risk assessments of antimony (Sb) in sediments of the Three Gorges Reservoir in China. Sci Total Environ 660:1433–1440. https://doi.org/10.1016/j.scitotenv.2019.01.014

Yan R, Qiu Z, Bian X, Yang J, Lyu S, Zhou A (2020) Effective adsorption of antimony from aqueous solution by cerium hydroxide loaded on Y-tape molecular sieve adsorbent: performance and mechanism. Colloids Surfaces A Physicochem Eng Asp 604:125317. https://doi.org/10.1016/j.colsurfa.2020.125317

Zhao Z, Wang X, Zhao C, Zhu X, du S (2010) Adsorption and desorption of antimony acetate on sodium montmorillonite. J Colloid Interface Sci 345:154–159. https://doi.org/10.1016/j.jcis.2010.01.054